Adjustment From Temperature Annual Dynamics for Reconstructing Land Surface Temperature Based on Downscaled Microwave Observations

Kangning Li, Yunhao Chen, Haiping Xia, Adu Gong, and Zheng Guo

***Abstract*—Land surface temperature (LST) is crucial to wide varieties of environmental issues, whereas its low tolerance to cloud contamination greatly challenges its applications. Passive microwave (PMW) measurements are employed to retrieve LST due to its great capability of penetrating clouds. Despite great efforts from previous studies, their further applications are limited by coarse resolution of PMW, uncertainty from cloudy coverage, and less attention on large-scale applications. To address these problems, this article proposes a method combining adjustment from annual temperature circle to reconstruct LST based on downscaled microwave observations over mainland China. In order to conduct a comprehensive and solid accuracy evaluation, the proposed method is validated according to three strategies namely comparing with moderate resolution imaging spectroradiometer (MODIS) LST, ground surface temperature, and *in situ* observations from the Heihe Watershed Allied Telemetry Experimental Research, respectively. In the strategy 1, mean root mean square error (RMSE) of predicted LST is 2.39 K and 1.33 K at day and night. According to the strategy 2, mean RMSE of MODIS, predicted and merged LST is 4.97 K, 5.07 K, and 4.93 K at daytime, and 2.32 K, 4.57 K, and 3.39 K at nighttime. In the strategy 3, they are 3.75 K, 3.90 K, and 2.87 K at day, and 2.80 K, 3.61 K, and 2.79 K at night. Furthermore, adjustments from annual temperature cycle are discussed. The proposed method is promising in future research for reconstructing LST with high spatiotemporal resolution at large scales thanks to its simple process, high accuracy, and seamless reconstruction.**

***Index Terms*—Annual temperature cycle (ATC), downscaling, land surface temperature (LST), passive microwave (PMW).**

Manuscript received May 23, 2020; revised July 19, 2020 and August 13, 2020; accepted August 22, 2020. Date of publication September 3, 2020; date of current version September 17, 2020. This work was supported in part by the Beijing Natural Science Foundation under Grant 8192025, in part by the National Natural Science Foundation of China under Grant 41771448, in part by the Science and Technology Plans of Ministry of Housing and Urban-Rural Development of the People's Republic of China and Opening Projects of Beijing Advanced Innovation Center for Future Urban Design, Beijing University of Civil Engineering and Architecture under Grant UDC2019031321 and Grant UDC201650100, and in part by the Beijing Laboratory of Water Resources Security and Beijing Key Laboratory of Environmental Remote Sensing and Digital Cities. *(Corresponding author: Yunhao Chen.)*

Kangning Li, Yunhao Chen, Haiping Xia, and Adu Gong are with the Beijing Key Laboratory of Environmental Remote Sensing and Digital Cities, Faculty of Geographical Science, Beijing Normal University, Beijing 100875, China, and also with the State Key Laboratory of Remote Sensing Science, Faculty of Geographical Science, Beijing Normal University, Beijing 100875, China (e-mail: lknkiki@mail.bnu.edu.cn; cyh@bnu.edu.cn; xiahp93@mail.bnu.edu.cn; gad@bnu.edu.cn).

Zheng Guo is with the National Satellite Meteorological Center, Beijing 100081, China (e-mail: guozheng@cma.gov.cn).

Digital Object Identifier 10.1109/JSTARS.2020.3021386

I. Introduction

LAND surface temperature (LST), a thermodynamic skin temperature of the earth surface routinely observed from remote sensing technology, is a key weather and climate variable closely associated with surface energy budget and water balance of the Earth system [1], [2]. It has been extensively employed in varieties of research fields including climate change, evapotranspiration, agricultural monitoring, urban heat island, fire detection, and public health [3]–[9]. Also, it has been widely recognized as a fundamental parameter for simulation models in the fields of hydrology, climatology, ecology, and meteorology [10]–[13].

LST experiences considerable spatiotemporal variations due to period-varying solar radiation, inconstant atmospheric conditions, and heterogeneous land surface characteristics [14]. Accurate LST measurements require capturing its spatial distribution and temporal dynamics [1]. These requirements are difficult for ground-based LST measurements, which cannot practically provide continuous large-scale observations. Instead, development of remote sensing technology especially thermal infrared (TIR) satellite makes it possible to observe LST with relatively high spatiotemporal resolution from regional to global scales. Moderate resolution imaging spectroradiometer (MODIS) LST products, thanks to their four-time global coverage per day and long-time available history, have been one of the most popular LST datasets, especially in large-scale and time-series studies [15]. However, a major shortcoming of TIR measurements is their low tolerance to cloud contamination and atmospheric conditions [16]. This sensitivity to clouds and incapacity to deal with cloudy pixels [17] lead to more than one-half of LST unavailable [2], which greatly challenges practical applications of TIR LST particularly when high spatiotemporal resolution is indispensable [16], [18], [19]. Therefore, accurate and practical methods for reconstructing seamless LST are highly desirable.

Some previous studies have attempted to reconstruct missing LST for its further practical applications, which can be generally grouped into three major categories namely spatiotemporal interpolation, model simulation, and data fusion. Methods based on spatial-temporal interpolation reconstruct missing LST with spatially neighboring, temporally nearest or spatiotemporal adjacent cloud-free pixels [15], [20], [21]. Model-driven methods are proposed mainly based on physical (or sometimes statistical) models with capability of delineating spatiotemporal variations

of LST to predict missing values under cloudy coverage [18]. Especially, annual temperature cycle (ATC) models based on LST temporal structure are good at estimating missing data even when large spatiotemporal gap existing [13], [18]. However, spatiotemporal interpolation and model simulation methods, with exclusive usage of TIR LST, are only an approximation of the theoretical clear-sky LST rather than an estimation of actual cloudy LST [2], [22]. Long *et al.* [22] combined the enhanced spatial and temporal adaptive reflectance fusion model and a bias correction approach to propose a data fusion method for all-weather LST generation at local scale.

Fusion methods with auxiliary data of passive microwave (PMW) are proved as promising ways for all-weather LST reconstruction [2], [16]. PMW measurements are proposed to estimate LST especially under cloudy sky, due to their much less sensibility to atmospheric absorption than TIR observations [23]. Kou *et al.* [24] and Xu *et al.* [25] presented a Bayesian maximum entropy (BME) method to predict LST by merging MODIS and advanced microwave scanning radiometer (AMSR-E) data. Holmes *et al.* [26] identified structural difference of DTC timing between PMW Ka-band and TIR, and then integrated them with independent random errors to enhance LST generation [27]. Duan *et al.* [2] developed a framework based on linear mixing model to reconstruct all-weather LST. Zhang *et al.* [16] proposed a method based on temporal component decomposition to estimate LST, which is a practical way to reconstruct 1-km all-weather LST at regional scale. Additionally, a mass of previous studies have already explored the potential of empirical methods based on relationship between PMW and temperature to estimate LST [28]–[34], especially when some physical or complex methods are not applicable.

Despite of these efforts, there are three limitations hampering their applications and requiring further investigations. First, despite of great amount of methods proposed to estimate LST based on PMW, unavailability of high-quality auxiliary, and complexity of calculation process make them inapplicable. On the contrary, relationship between PMW and temperature taking advantages of its simplicity and high accuracy is promising for estimate LST. This relationship depends on LST information with great effects from spatiotemporal variations of cloudy coverage. Annual temperature dynamics with capacity of providing stable spatial and temporal information are employed to compensate this uncertainty. Second, coarse resolution of microwave observations with mixture weather information certainly brings difficulties to reconstruct high-resolution LST. Besides, deficiency PMW, due to satellite orbit growing from the North Pole (the same as the South Pole) to the equator with approximately triangle gap, also challenges data applications at large scales. Third, despite of great spatiotemporal variations of missing LST at large scales [2], [16], most previous methods were conducted at local or regional scales. As less attention has been paid on high proportion of cloudy coverage and its considerable spatiotemporal variations, especially nearby the equator, method feasibility at large scales remains largely unknown.

To tackle these problems, this study develops a method by combining adjustment from annual temperature model to reconstruct LST from downscaled microwave measurements over mainland China. Additionally, adjustments from annual temperature dynamics are further discussed to better understand the proposed method. This study potentially provides an accurate and efficient way to estimate seamless LST based on microwave observations, and supports for further associated applications at large scales. Generally, this article is organized as: Section 1 briefly introduces the background; Section 2 represents the study area and data; Section 3 describes the methodology; and Sections 4 and 5 demonstrate results and discussion, respectively.

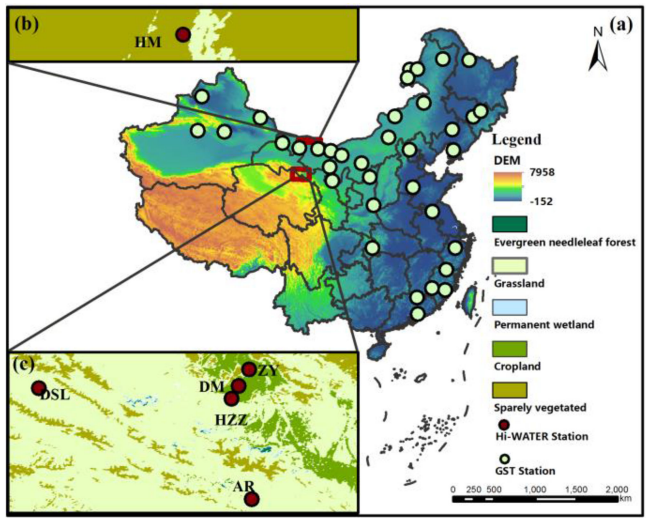

Fig. 1. Study area across mainland China with distributions of ground surface temperature (GST) stations (a) and *in situ* stations from the Heihe Watershed Allied Telemetry Experimental Research (HiWATER) (b and c). The background of (a) is DEM and the background of (b and c) is MODIS LULC, in 2018.

II. Study Area and Data

A. Study Area

Mainland China (3°51′ N-53°33′ N, 73°33′ E-135°05′ E), covering a vast territory with considerable varieties of climate zones, is selected as the study area [see Fig. 1(a)]. Before introducing the method, it is necessary to analyze spatial-temporal variations of missing LST across the study area for providing fundamental information of further accuracy validation and discussion. In Fig. 2, missing LST is explored from three respects including spatial distributions, statistics analysis, and seasonal variations. Missing LST shows a large amount of missing days in a year and considerable spatiotemporal variations with evident north–south contrasts at both daytime and nighttime. According to region characteristics and spatial variations of cloudy coverage, the study area is divided into four parts for further process. In the statistics analysis of probability density function (PDF) and cumulative distribution function (CDF), over 50% of pixels suffer from cloudy coverage during more than 200 d in a year. Additionally, deficiency of data is found strong seasonal variations with descending order as summer (JJA), spring (MAM), winter (DJF), and autumn (SON). Missing LST with not only large amount but also great spatial-temporal variations strongly challenges LST reconstruction and applications. Generally, north–south temperature gradient [36] and considerable

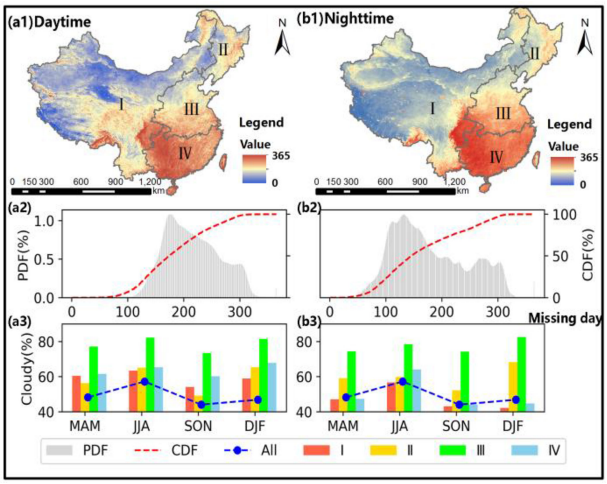

Fig. 2. Spatiotemporal variations of missing LST caused by cloudy coverage at daytime (a) and nighttime (b). Spatial variations of missing LST are shown by missing days of a year in every pixel across the study area (a1 and b1). Value distributions of missing days in a year are shown by PDF and CDF (a2 and b2). Seasonal variations of cloudy coverage are shown in a3 and b3.

spatiotemporal variations of cloudy coverage make China an ideal study area to examine potential and availability of the proposed method.

B. Data

1) Data for the Method: Aqua MODIS daily LST products named MYD11A1 (collection 6) in the year of 2018 are employed as satellite TIR LST data. MODIS LST products are retrieved based on the generalization split-windows LST algorithm [37] by utilizing cloud-free measurements at approximately 1:30 and 13:30 local solar time. Wan [38] reported that retrieval errors of MODIS LST were mostly less than 1 K and root mean square errors (RMSE) were less than 0.5 K. Furthermore, Wan [39] proved the mean error of collection 6 LST was within 0.6 K and Duan *et al.* [10] found that collection 6 outperformed the corresponding collection 5 LST products over most desert sites.

PMW measurements are collected from AMSR-2 on Global Change Observation Mission 1st-Water (GCOM-W1) satellite, which passes over at approximately 1:30 and 13:30 local solar time (similar to MODIS Aqua). AMSR-2 level 2A daily BTs at 10 km in 2018 are collected from G-Portal, a portal system allowing users to search, and download products derived by Japan Aerospace Exploration Agency's (JAXA's) Earth observation satellite. Given characteristics and correlation of all channels [27], [40], 06, 37, and 89 GHz vertical channels are selected to balance accuracy and efficiency.

Skin temperature (SKT), instantaneously responding to changes of surface fluxes, is collected from ERA5-Land hourly $0.1\,^{\circ}\times 0.1\,^{\circ}$ climate reanalysis dataset to compensate information about background climate. To better match the overpass time of MODIS, SKT data are average between 13:00 and 14:00 at daytime (average between 1:00 and 2:00 at nighttime). SKT data are available on the European Centre for Medium-Range Weather Forecasts (ECMWF).[1] Balsamo *et al.* [41] reported that ERA-5 data were qualified for various applications and they were notably improved with higher spatiotemporal resolution comparing to the previous version (ERA-Interim).

TABLE I
INFORMATION ABOUT DATA EMPLOYED IN THE PROPOSED METHOD

Name	Product	Number of data	Temporal/spatial resolution
LST	MYD11A1	365×2	Daily twice /1 km
PMW	AMSR-2 L3	365×2×3	Daily twice /10 km
SKT	ERA5-Land	365×2	Hourly /10 km
NDVI	MYD12A2	22	16-day/ 1 km

In number of data, 365 represents the number of days in the year, 2 represents twice a day (daytime and nighttime), 3 represents channel amount of PMW, and 22 represents number of 16-day NDVI in a year. It is noted that spatial resolution here is spatial sampling of the products.

Normalized difference vegetation index (NDVI) was collected from MODIS Aqua Vegetation indices 16-d 1-km MYD12A2, in order to provide phenology and spatial information. MODIS NDVI is available at EARTHDATA. Data details are presented in Table I.

2) Data for Validation: Ground surface temperature (GST) products are collected from hourly observation dataset of China's automatic weather stations. These datasets are available at the National Meteorological Data Center.[2] Since previous studies proved availability of GST in studies of temperature validations and urban heat island [42], this article employed it as validation data. A total of 36 stations are selected due to its capability of GST measurements and relatively wide distributions [see Fig. 1(a)].

Six ground-based stations [see Fig. 1(b) and (c)] are utilized to validate the accuracy of the proposed method. These stations are from the HiWATER. Four-component radiometer sets provide average values at every 10 min. Since HiWATER observations have been widely employed in previous studies to validate LST [2], [10], [43], [44], *in situ* measurements are qualified for accuracy evaluation. Detailed information about geographic location and descriptions of these selected sites is shown in Table II.

III. METHODOLOGY

The proposed method can be generally divided into three major steps including PMW downscaling, ATC model, and LST estimation. To clearly introduce the method, flowchart is provided in Fig. 3.

Before these major steps, different kinds of data employed in the method need data preprocessing to make them ready for the following processes. Data (presented in Table I) from different coordinate systems are transformed to the same projection. SKT is resampled to 1 km by the nearest neighbor method. MODIS LST with flags of "average LST error $>$ 3 K" is eliminated to avoid cloud contamination as far as possible. MODIS LST is

[1][Online]. Available: https://www.ecmwf.int/
[2][Online]. Available: http://data.cma.cn/site/index.html

TABLE II
INFORMATION ABOUT SLEETED HIWATER SITES

Name	Abbreviation	Longitude	Latitude	Elevation (m)	Radiometer Set			Land cover
					Instrument	Height (m)	Diameter of FOV (m)	
Dashalong	DSL	98° 56′E	38°50′ N	3739	CNR1	6	44.8	Swamp meadow
Huangmo	HM	100°59′E	42°06′N	1054	CNR1	6	44.8	Desert steppe
Huazhaizi	HZZ	100°19′E	38°46′N	1731	CNR1	6	44.8	Desert steppe
Zhangye	ZY	100°26′E	38 °58′N	1460	CNR1	6	44.8	Reed
A'rou	AR	100°27′E	38°02′N	3033	CNR4	5	37.3	Alpine meadow
Daman	DM	100°22′E	38°51′N	1556	Epply PSP&PIR	12	89.6	Cropland

FOV is acronym for field of view.

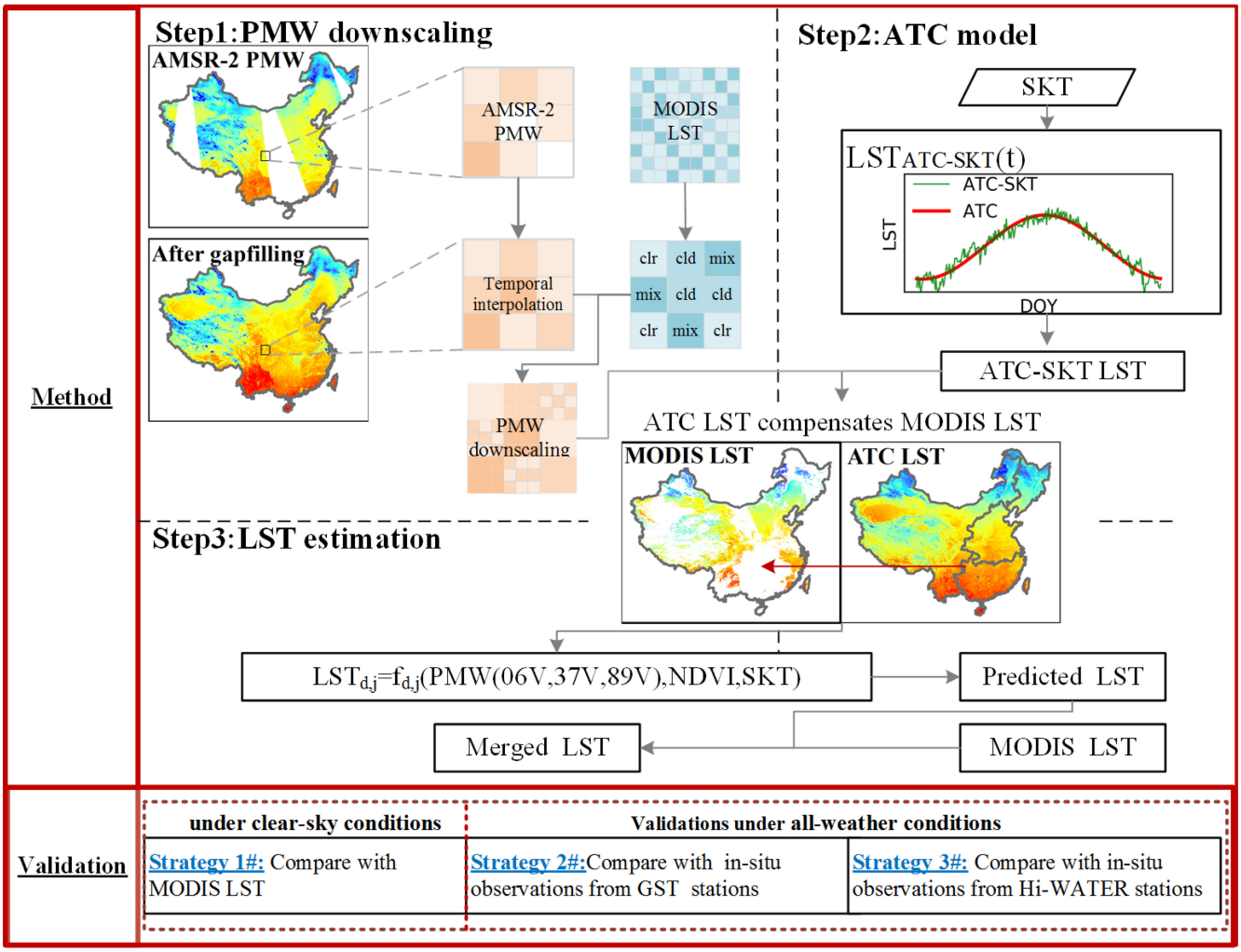

Fig. 3. Flowchart of the proposed method including two parts namely method and validation.

flagged as clear and cloudy conditions according to its quality control.

A. PMW Downscaling

PMW downscaling aims to improve spatial resolution and decompose mixture weather information by distinguishing subpixel weather condition in 10-km PMW. It can be divided into three steps namely temporal interpolation, condition mask, and mixture decomposing. Temporal interpolation is employed to conduct gapfilling on AMSR-2 PMW. Condition mask and mixture decomposing are designed to estimate subpixel PMW based on their weather conditions.

First, temporal interpolation, a gapfilling method based on values of their neighboring days [15] [see (1)], is conducted on

missing PMW resulted from orbit trajectory. Neglect of missing PMW in some previous studies was likely to bring uncertainty and inapplicability to large-area studies. In addition, 6, 37, and 89 GHz V (vertical) polarized channels are selected in the method according to microwave characteristics. A total of 37 GHz V is reported as the best microwave channel for all-weather LST retrieval [29].

$$\mathrm{PMW}_{f,d,m} = \mathrm{Mean}\left(\mathrm{PMW}_{f,d-n,m},\ \mathrm{PMW}_{f,d+n,m}\right) \quad f \in \{6, 37, 89\} \tag{1}$$

where f is the frequency of microwave (6, 37, 89 GHz V), d is the DOY (day of the year), m is the location of missing PMW, $n = 1$ is employed as temporal interval of gapfilling. If there are missing values remaining after first gapfilling, $n = 2$ is employed (after experiments, only a few pixels need this temporal expand). Note that 1st and 365th days are reconstructed by its adjacent days.

Second, PMW condition mask (3) is conducted based on clear-sky percentage of 10-km MODIS and quality flags of 1-km MODIS LST. Percentage of clear-sky condition (PC) is calculated according to (2). To address mixture weather information in 10-km PMW pixels, $\mathrm{PMW}_{10\mathrm{km}}$ is first divided into three weather categories namely clear (PC = 1), cloudy (PC = 0), and mixed [PC∈(0,1)] pixels. And then, mixed PMW pixels are further divided into pure clear-sky ($\mathrm{PMW}_{\mathrm{mix\text{-}clr},1\mathrm{km}}$) and cloudy-sky ($\mathrm{PMW}_{\mathrm{mix\text{-}cld},1\mathrm{km}}$) pixels according to quality flags of 1-km MODIS LST.

$$\mathrm{PC}_{d,i} = \frac{N_{\mathrm{MODIS-clr},d,i}}{N_i} \tag{2}$$

where $\mathrm{PC}_{d,i}$ is the percentage of clear-sky condition on the ith pixel of $\mathrm{PMW}_{10\mathrm{km}}$ in the dth day. $N_{\mathrm{MODIS\text{-}clr},i}$ is number of MODIS LST with flag of clear-sky. N_i is number of MODIS $\mathrm{LST}_{1\mathrm{km}}$ in the pixel of $\mathrm{PMW}_{10\mathrm{km}}$.

$$\mathrm{PMW}_{1\mathrm{km},d,i} = \begin{cases} \mathrm{PMW}_{\mathrm{clr},1\mathrm{km},d,i}\ \mathrm{PC}_{d,i} = 1 \\ \mathrm{PMW}_{\mathrm{cld},1\mathrm{km},d,i}\ \mathrm{PC}_{d,i} = 0 \\ \begin{cases} \mathrm{PMW}_{\mathrm{mix-clr},1\mathrm{km},d,i}\ (\mathrm{PC}_{d,i} \in (0,1)) \cap (M \in \{\mathrm{clr}\}) \\ \mathrm{PMW}_{\mathrm{mix-cld},1\mathrm{km},d,i}\ (\mathrm{PC}_{d,i} \in (0,1)) \cap (M \in \{\mathrm{cld}\}) \end{cases} \end{cases} \tag{3}$$

where $\mathrm{PMW}_{1\mathrm{km},d,i}$ represents 1-km downscaled PMW in the ith pixel on the dth day. $\mathrm{PMW}_{\mathrm{clr},1\mathrm{km},d,i}$ and $\mathrm{PMW}_{\mathrm{cld},1\mathrm{km},d,i}$ are resample results from 10-km $\mathrm{PMW}_{\mathrm{clr}}$ and $\mathrm{PMW}_{\mathrm{cld}}$. M∈{clr} or {cld} represents weather condition from quality flags of 1-km MODIS LST.

Third, inspiring from the liner spectral mixture model [45] and decomposition of subpixel temperature under different weather conditions [2], the process of decomposing mixture information is proposed based on subpixel decomposition. In other words, mixed $\mathrm{PMW}_{10\mathrm{km}}$ is assumed as a linear combination (4) of $\mathrm{PMW}_{\mathrm{mix\text{-}clr},1\mathrm{km}}$ and $\mathrm{PMW}_{\mathrm{mix\text{-}cld},1\mathrm{km}}$. As difference between $\mathrm{PMW}_{\mathrm{mix\text{-}clr},1\mathrm{km}}$ and $\mathrm{PMW}_{\mathrm{mix\text{-}cld},1\mathrm{km}}$ is found relatively homogeneous during every season from statistical analysis, it is calculated as (6). $\mathrm{PMW}_{\mathrm{mix\text{-}clr},1\mathrm{km}}$ and $\mathrm{PMW}_{\mathrm{mix\text{-}cld},1\mathrm{km}}$ pixels estimated by using simultaneous (4) and (5) are the final results of the PMW downscaling. According to season definitions, spring includes March, April, and May (MAM), summer includes June, July, and August (JJA), autumn includes September, October, and November (SON), and winter includes December, January, and February (DJF).

$$\mathrm{PMW}_{10\mathrm{km},d,i} = \mathrm{PMW}_{\mathrm{mix-clr},1\mathrm{km},d,i} \times \mathrm{PC}_i + \mathrm{PMW}_{\mathrm{mix-cld},1\mathrm{km},d,i} \times (1 - \mathrm{PC}_{d,i}) \tag{4}$$

$$\mathrm{PMW}_{\mathrm{mix-cld},1\mathrm{km},d,i} = \mathrm{PMW}_{\mathrm{mix-clr},1\mathrm{km},d,i} + \Delta P_{s,i} \tag{5}$$

$$\Delta P_{s,i} = \left(\sum_{1}^{sd} (\mathrm{PMW}_{\mathrm{cld},10\mathrm{km},d,i} - \mathrm{PMW}_{\mathrm{clr},10\mathrm{km},d,i}\right) / sd \tag{6}$$

where $\triangle P_{s,i}$ is difference between $\mathrm{PMW}_{\mathrm{clr},10\mathrm{km}}$ and $\mathrm{PMW}_{\mathrm{cld},10\mathrm{km}}$ in the ith pixel during the season. sd represents number of days in every season. It is noted if there is no $\mathrm{PMW}_{\mathrm{clr},10\mathrm{km}}$ and $\mathrm{PMW}_{\mathrm{cld},10\mathrm{km}}$ in a season, $\triangle P_{s,i}$ is estimated by average of its neighbor seasons.

B. ATC Model

Since the ATC model with "semiphysical" nature is robust and stable especially when large spatiotemporal cloudy coverage exists [18], annual temperature dynamics are employed to provide information about temporal variations to LST estimation. Previous study reported that surface characters and meteorological conditions were helpful to provide weather fluctuations over the original ATC model [18], [46]. An enhanced ATC model (7) with auxiliary of SKT based on the hybrid framework of the ATC model [18] is employed. SKT is resampled to 1 km by the nearest neighbor method.

$$\begin{aligned} \mathrm{LST}_j(d) &= \varphi\left(T_{0,j}, A_j, \theta_j, t, \Delta T_{\mathrm{SKT}}(d), b_j\right) \\ &= T_{0,j} + A_j \sin\left(2\pi d^{-1} d + \theta_j\right) + b_j \Delta T_{\mathrm{SKT}}(d) \end{aligned} \tag{7}$$

where j is the pixel of images; d refers DOY; φ denotes the ATC functions; $T_{0,j}$, A_j, and θ_j are annual mean, amplitude, and phrase shift of ATC, respectively; and bj is the coefficient of ΔT_{SKT}(d). ΔT_{SKT}(d) is difference between observed and predicted SKT.

Since previous research reported relationship between observed and predicted SKT was similar to that between satellite-derived and predicted LST [47], SKT difference was utilized to compensate weather fluctuations.

$$\begin{aligned} \Delta T_{\mathrm{SKT}}(d) &= T_{\mathrm{SKT}}(d) \\ &- \varphi_{\mathrm{SKT}}\left(T_{\mathrm{SKT\_0},j}, A_{\mathrm{SKT\_}j}, \theta_{\mathrm{SKT\_}j}, d\right) \\ &= T_{\mathrm{SKT}}(d) - \left(T_{\mathrm{SKT\_0},j} + A_{\mathrm{SKT\_}j} \sin\left(2\pi d^{-1} d + \theta_{\mathrm{SKT\_}j}\right)\right) \end{aligned} \tag{8}$$

where T_{SKT} is reanalysis data of SKT; φ_{SKT} denotes the original ATC functions of SKT; and $T_{\mathrm{skt}\cdot 0,j}$, $A_{\mathrm{skt}\cdot j}$, and $\theta_{\mathrm{skt}\cdot j}$ refer annual mean, amplitude, and phrase shift of the ATC model based on SKT.

C. LST Estimation

LST estimation in the proposed method is based on the relationship between PMW and available MODIS LST. This relationship is possibly affected by availability of MODIS LST especially at large scales, since missing MODIS LST cannot be employed to model it. Taking the study area in this article as an example, there are large spatiotemporal variations of cloudy coverage (see Fig. 2) and great gradient of temperature from the north to south. Specifically, great percentage of missing MODIS LST caused by cloudy coverage especially in the southern regions is likely to bring uncertainty and biases to the relationship and LST estimation. Despite of wide applications of this relationship in LST estimation, less attention has been paid to potential biases resulted from considerable spatial-temporal variations of cloudy coverage and temperature gradient when modeling the relationship. To address this issue, temporal dynamics from ATC results are employed to make adjustment in the training process. In other words, ATC LST is used to compensate heterogeneous distributions of available MODIS LST. Training process is to build the relationship model between PMW and available MODIS LST. There are two main processes of LST estimation including adjustments of training samples with ATC, and estimation LST based on the random forest (RF) model.

In the adjustment process, it is necessary to introduce when and how to conduct adjustment from temporal dynamics. The objective of adjustment is to compensate uneven availability of MODIS LST in relationship modeling. Thus, rules for adjustment situations are shown as following: 1) percentage of missing MODIS LST is more than 70%; 2) there is a window of missing data covering more than 500×500 pixels. If one of these conditions occur, it is necessary to conduct adjustment based on ATC. In the proposed method, the study area is divided into four parts and every part is the object of condition test. Region division is mostly based on the spatial distributions of cloudy coverage [see Fig. 2 (a1) and (b1)] and temperature gradient across mainland China. Whether how to conduct region division depend on the aim of pursuing more homogeneous distributions of training samples. In other words, region division is not prerequisite and it depends on the characteristics of the study area. Missing percentage of 70% is not an invariant parameter, since it is based on statistics analysis and spatial distributions of missing data (see Fig. 2). Furthermore, adjustment is conducted by utilizing 2% of random pixels from ATC LST together with available MODIS LST in the process of modeling the relationship. ATC LST is employed to adjust biased distributions of available MODIS LST. Percentage of random pixels is selected based on the standards that this percentage can adjust data distributions and maintain statistical characteristics. As homogeneous distributions of LST are found more important than available percentage in the training process, determination of 70% or 2% is not a key point in the proposed method. A total of 70% and 2% are examples and suggestions rather than invariant parameter.

After adjustment for training samples, the RF model is employed to estimate LST. RF [48], a machine learning algorithm on the base of classification and regression tree, is utilized thanks to its robustness and stability. Hyperparameter optimizing is conducted based on grid search with data on the first day of every months to improve performance of the RF model. Grid search is guided by performance metrics to search a manually specified subset in the hyperparameter space of a learning algorithm. Since the RF model has been implemented in the Scikit-learn Python library, this method can be easily applied in further applications. Relationship between MODIS LST and related variables including PMW with three selected channels [29], SKT [18] and NDVI [18] [46] is modeled in the RF algorithm (9). Then, this modeled relationship is employed to estimate missing LST. Final results of the proposed method are merged from MODIS LST under clear-sky conditions and estimated LST under cloudy conditions.

$$\mathrm{LST}_{d,j} = f_{\mathrm{RF}-d}\left(\mathrm{PMW}_{d,j}\left(6\mathrm{V},37\mathrm{V},89\mathrm{V}\right),\mathrm{SKT}_{d,j},\mathrm{NDVI}_{\frac{j}{16}}\right) \quad (9)$$

where d refers DOY; j represents the pixel of images.

D. Validation

To conduct comprehensive accuracy validations, three strategies are chosen to evaluate results of the proposed method. There are several reasons for selecting these validation strategies. First, MODIS LST with relatively wide distributions and large amount is employed to test whether MODIS and estimated LST are consistent. Second, GST taking advantages of its wide distribution and comparably large amounts is employed to compensate local distributions of six stations from HiWATER. Third, observations with all-weather measurements are recognized as a popular way for accuracy evaluation in previous studies [2], [10], [16], [18]. Information about validation strategies is also provided in Fig. 3.

Strategy 1: Under clear-sky conditions, MODIS LST is employed to validate consistency between it and the predicted temperature. This predicted LST utilized in the strategy 1 is estimated from the proposed method under cloud-free conditions. It is noted that clear-sky predicted LST is only used in validation but not in merged LST.

Strategy 2: GST is 0-cm SKT measured by thermometer. After spatial and temporal match, GST is utilized to compare with MODIS LST under clear-sky conditions and estimated LST under cloudy conditions.

Strategy 3: Six observation sites with all-weather measurements from HiWATER are employed. According to Zhang *et al*. [16], ground-based LST from the station within 1-km homogenous pixels is capable of representing 1-km LST. These six stations within the 1-km pixel contain homogenous land cover according to MCD12Q1. To ensure temporal match, in situ data measured at 1:30 and 13:30 local solar time (approximately overpass time of MODIS Aqua and AMSR-2) are collected in validations. Their observed LST is estimated (10) with Surface longwave upward and downward radiation (LWUR and LWDR). LWUR and LWDR are collected from the four-component radiometer in every station

$$\mathrm{LST}_{in\ situ} = \left(\frac{\mathrm{LWUR} - \mathrm{LWDR}\times(1-\epsilon_B)}{\sigma\epsilon_B}\right)^{1/4} \quad (10)$$

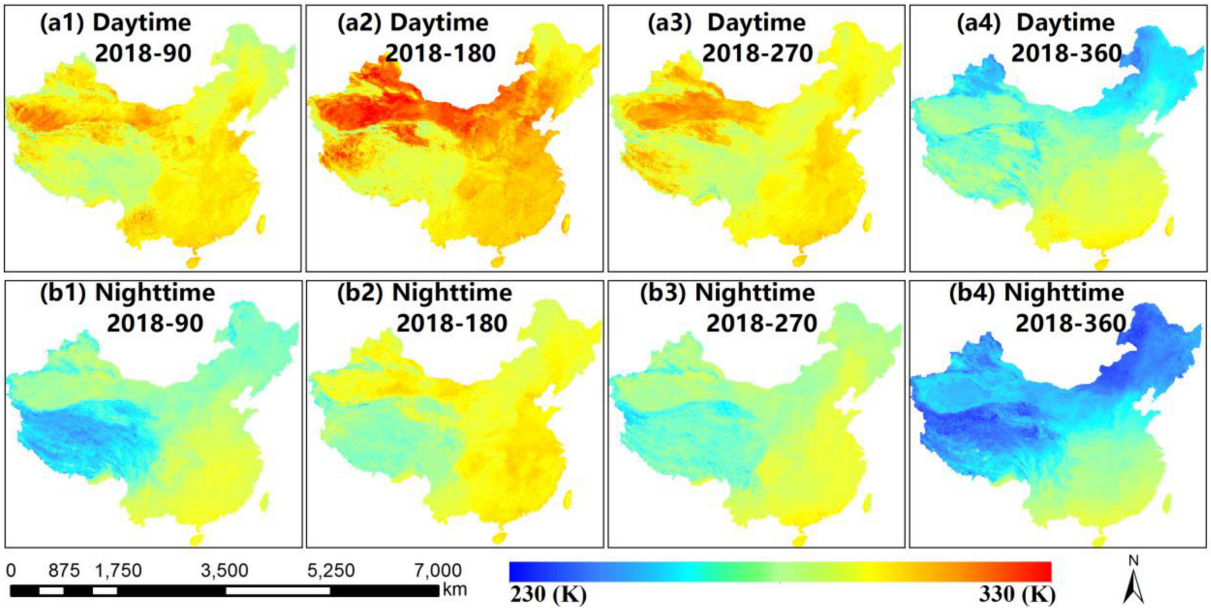

Fig. 4. Results of the proposed method across mainland China on the 90th, 180th, 270th, and 360th day of the year at daytime (a) and nighttime (b).

here, LST_{insitu} is observed LST; ε_{B} is the broadband surface emissivity; σ is the Stefan–Boltzmann constant (5.67×10^{-8} $\mathrm{W/m^2/K^4}$).

IV. Results

A. Spatial Performance

Fig. 4 shows spatial distributions of results in the proposed method during daytime and nighttime. The 90th, 180th, 270th, and 360th day of the year are taken as example to represent spatial performance during spring, summer, autumn, and winter, respectively. At daytime, high temperature in the northwest is observed in the first three seasons, which is possibly attributed to environment of arid areas and less cloudy coverage in the northwest area [2]. At nighttime, greater north–south contrasts are found in all four seasons. Locations of higher temperature at nighttime are consistent to spatial distributions of cloudy coverage [see Fig. 2], which suggests clouds can make heat preservation by increasing downward longwave radiation at night. Generally, the proposed method is capable of reconstructing spatiotemporal variations of LST with relatively high spatial resolution at both daytime and nighttime. Further quantitative validations are conducted in the next part.

B. Accuracy Validations

To conduct a comprehensive and solid accuracy evaluation, three aforementioned strategies are employed to validate the proposed method.

According to the strategy 1, the present method is evaluated by two accuracy indicators namely RMSE and mean absolute error under clear-sky conditions [see Fig. 5]. Mean RMSE is 2.39 K and 1.33 K at daytime and nighttime, respectively, which shows consistency between results of the proposed method and

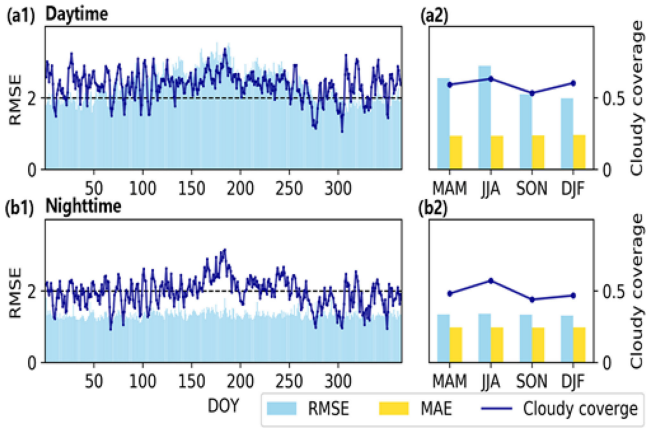

Fig. 5. Accuracy validations of the proposed method according to the strategy 1 at daytime (a) and nighttime (b). RMSE (the right axe) and cloudy coverage (the left axe) are shown in the annual (a1 and b1) and seasonal variations (a2 and b2).

MODIS LST. Moreover, accuracy validations are conducted from the respect of seasonal variations to further explore the performance and its relationship with cloudy coverage. Great correlation between RMSE and percentage of cloudy coverage is found at daytime, while less correlation between RMSE and weather conditions is found at night. This difference is possibly attributed to different contribution of cloudy coverage to temperature between daytime and nighttime. Comparing with RMSE at daytime, less seasonal variations are observed at night. Comparatively high and stable accuracy at nighttime indicates that performance of the method is found better at night than day. Generally, the proposed method is validated as an accurate way with consistency to MODIS LST according to the strategy 1.

According to the strategy 2, performance of the method is evaluated by comparing with GST from selected stations across

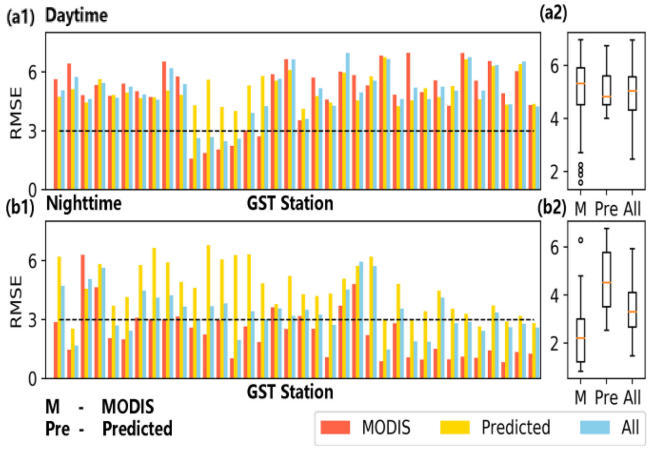

Fig. 6. Accuracy validations of the proposed method according to the strategy 2 at daytime (a) and nighttime (b), respectively. Bar plots are RMSE at every GST station, and box plots are RMSE under three conditions. "M" represents MODIS LST, "Pre" represents predicted LST, and "All" represents merged LST.

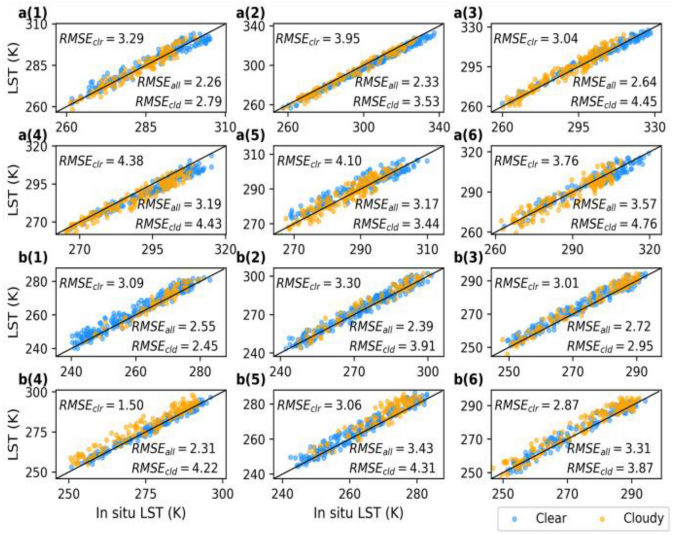

Fig. 7. Accuracy validations of the proposed method according to the strategy 3 at daytime (a) and nighttime (b), respectively. Scatter plots of the predicted LST and observed LST at the six selected sites namely DSL (a1 and b1), HM (a2 and b2), HZZ (a3 and b3), ZY (a4 and b4), AR (a5 and b5), and DM (a6 and b6) under all-weather conditions.

mainland China [see Fig. 6]. GST is employed to compare with MODIS, predicted and merged LST, respectively. Accuracy of MODIS LST is recognized the reference of difference between thermometer-derived soil temperature and satellite-derived temperature. Thus, relative accuracy conducted by comparing accuracy between MODIS LST under clear-sky and predicted LST under cloudy-sky is as important as it absolute value. Since merged LST is the final result of the proposed method, comparisons between it and GST under all-weather conditions are necessary. At daytime, mean RMSE between MODIS LST and GST under cloudy-free conditions is 4.97 K, and mean RMSE of predicted LST under overcast conditions is 5.07 K. Mean RMSE of merged LST under all-weather conditions is 4.93 K at daytime. At nighttime, mean RMSE under these three conditions is 2.32 K, 4.57 K, and 3.39 K, respectively. Comparable RMSE of MODIS and predicted LST can prove accuracy and consistency of the proposed method. Additionally, lower nighttime RMSE than daytime one in all three conditions indicates that the method works better at night. By comparing with GST, the proposed method is validated as an accurate way for temperature reconstruction.

According to the strategy 3, the proposed method is validated by in situ observations from HiWATER under all-weather conditions [see Fig. 7]. Similar to the strategy 2, *in situ* observations are employed to compare with MODIS LST under clear-sky conditions, predicted LST under cloudy conditions, and merged LST under all-weather conditions, respectively. Strong correlation between predicted and validation LST is observed from scatter plots. Under cloud-free conditions, mean RMSE of MODIS LST is 3.75 and 2.80 K at daytime and nighttime, respectively. Under cloudy conditions, mean RMSE of predicted LST is 3.90 K at day and 3.61 K at night. Mean RMSE of merged LST under all-weather conditions is 2.87 and 2.79 K during day and night, respectively. Lower RMSE at nighttime under all-weather conditions is possibly due to less LST variations at night. RMSE of MODIS LST here is larger than 1 K reported by Wan [38], because their validations were conducted on the condition of best-quality MODIS LST and well-chosen measurements [10]. Accuracy evaluation of MODIS LST under clear-sky conditions can be approximately recognized as reference of systematic bias between satellite-derived and ground-observed LST, as Duan, *et al.* [10] reported systematic bias (-3.44 K) between the C6 MODIS LST and observed LST. Previous research reported several reasons for this systematic bias, namely uncertainty from instrument measurements, difficulty of emissivity estimation, spatial inconsistency, and spatiotemporal mismatch [2], [10]. Despite of these limitations, *in situ* observations are widely applied in LST validations especially under overcast conditions. By taking RMSE of MODIS as reference, systematic bias accounts for the majority of RMSE. Except for this, larger RMSE of predicted LST than that of MODIS LST is possibly attributed to method error and complex weather background of overcast. Besides, the proposed method might be advanced with further improvement on gapfilling of PMW, and spatiotemporal match of data sources including MODIS LST, AMSR-2 PMW, and SKT. To sum up, the proposed method is a promising and accurate way for reconstructing seamless daily LST after comprehensive validations according to the aforementioned three strategies.

V. Discussion

Statistical methods based on PMW for LST estimation are extensively applied owing to its great simplicity and efficiency, especially when physical methods are not applicable [23], [28], [29], [32], [34], [49]. However, statistical methods are possibly affected by considerable spatial-temporal variations of cloudy coverage, because they are based on the relationship between PMW and available LST. As aforementioned, missing data show great spatial and temporal variations with evident north–south contrasts. These contrasts and evident north-south temperature

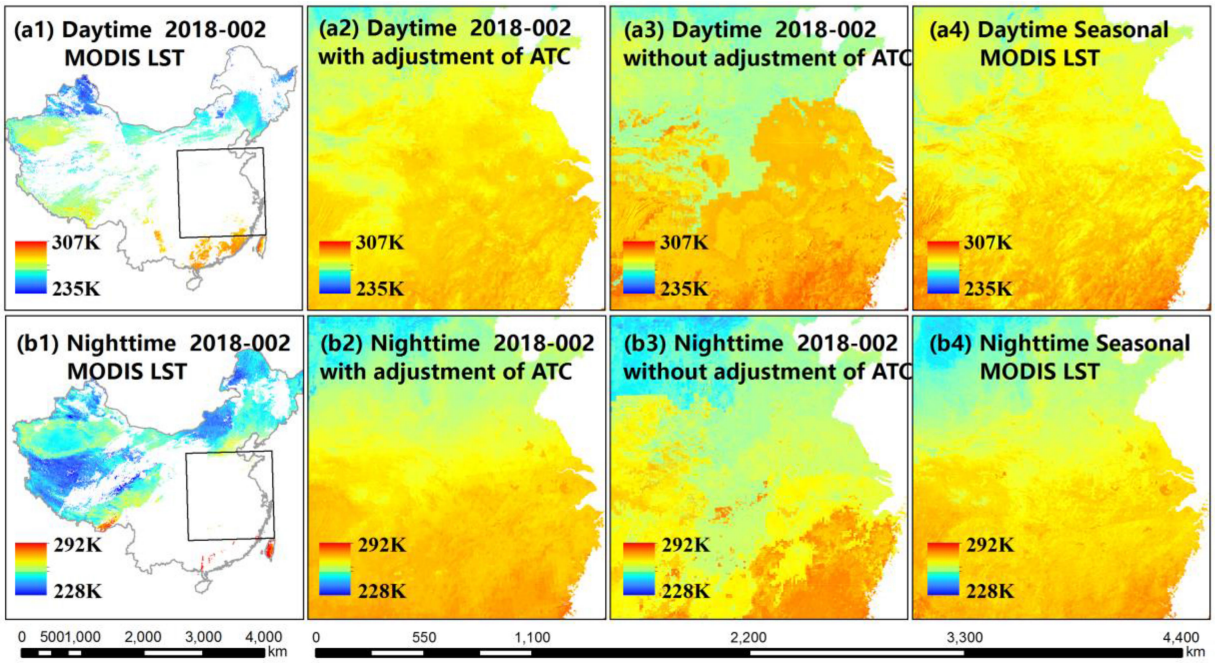

Fig. 8. Comparisons of spatial distributions between LST estimation with and without adjustment from ATC during daytime (a) and nighttime (b) according to seasonal MODIS LST.

gradient [36] are likely to bring uncertainty and even bias to statistical models. To address this problem, the ATC model with "semiphysical" nature [18] is employed in the proposed method for adjustment.

To clearly show improvements of adjustment from annual temperature dynamics, comparisons between the proposed method (with adjustment from ATC) and LST estimation without adjustment from ATC are conducted. From the aspect of qualitative comparisons, spatial distributions of results from those two methods are shown in Fig. 8. Seasonal aggregation of MODIS LST is taken as reference in the comparisons due to its seamless and clear spatial variations. The 2nd day of the year is taken as example due to its typical spatial distributions of cloudy coverage. Results of the proposed method are observed not only similar LST spatial distributions and variations but also approximately spatial resolution to 1-km MODIS LST at both daytime and nighttime. The present method overcomes coarse spatial resolution and low accuracy of subsurface temperature from physical methods [2], [8], [23], [50]. On the contrary, results of LST estimation without adjustment from ATC show evidently different spatial distributions and less spatial variations compared to the reference data. This uncertainty and bias are attributed to considerable north–south contrasts of cloudy coverage, especially in large-scale studies. With adjustments from annual temperature dynamics, the proposed method is capable of capturing spatial variations of temperature with high spatial resolution. Additionally, these adjustments are potential to improve spatial accuracy of other empirical-based methods for LST estimation.

Furthermore, comparisons are conducted from quantitative aspects by validating with GST and in situ LST from HiWATER

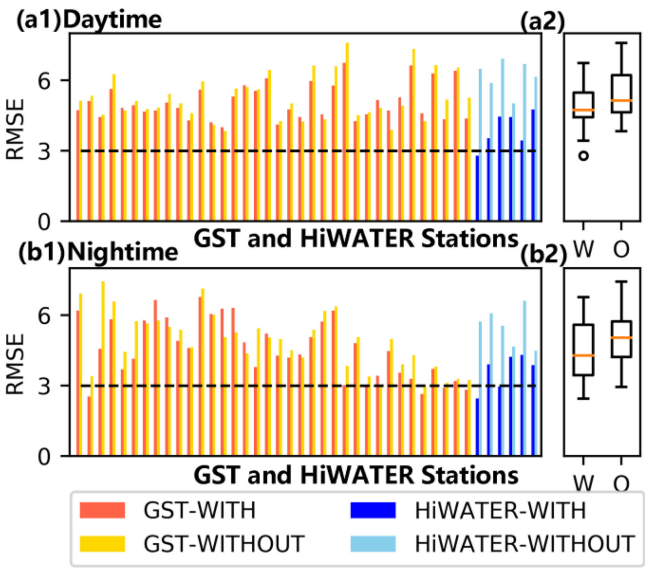

Fig. 9. Accuracy comparisons between the LST estimation with (W in the figure) and without (O in the figure) adjustment from ATC at daytime (a) and nighttime (b), respectively. Bar plots are RMSE at GST and HiWATER stations (a1 and b1) and box plots are RMSE of these two methods (a2 and b2).

[see Fig. 9]. According to the strategy 2, mean RMSE of the proposed method is 5.07 K and LST estimation without adjustment from ATC is 5.26 K at daytime. They are 4.57 K and 4.89 K at night, respectively. Despite of relatively small difference, the proposed method with adjustment from ATC shows lower RMSE than that without adjustment at almost all GST stations during both day and night. According to the strategy 3 by validating with *in situ* observations from HiWATER, mean RMSE of the

LST estimation with and without adjustment from ATC is 3.90 K and 6.19 K at day, 3.61 K, and 5.51 K at night. With adjustment from ATC, accuracy of the proposed method is greatly improved. To sum up, adjustments from annual temperature dynamics can improve spatial resolution and accuracy of the proposed method and it is promising in further applications of other empirical estimation methods.

VI. Conclusion

Wide applications of TIR LST are greatly challenged by its low tolerance to atmospheric conditions. As PMW is capable of penetrating clouds, previous studies reported that PMW data are promising for reconstructing seamless LST. Although great amount of temperature estimation methods based on PMW observations are proposed, several limitations remain hampering their accuracy and applications. To address these problems, this article proposes a method by combining adjustment from annual temperature dynamics to reconstruct LT based on downscaled microwave measurements over mainland China.

The proposed method is validated through three strategies for comprehensive and solid accuracy evaluation. According to the strategy 1, by comparing with MODIS LST, mean RMSE of the predicted LST is 2.39 and 1.33 K at daytime and nighttime, respectively. In the strategy 2, by comparing with GST, mean RMSE of MODIS LST under clear sky, predicted LST under cloudy sky and merged LST under all-weather conditions is 4.97 K, 5.07 K, and 4.93 K, respectively, at daytime. At night, mean RMSE under these three conditions is 2.32 K, 4.57 K, and 3.39 K. According to the strategy 3, mean RMSE of MODIS, predicted and merged LST under three weather conditions is 3.75 K, 3.9 K, and 2.87 K at daytime, and 2.80 K, 3.61 K, and 2.79 K at nighttime. After these three comprehensive validation strategies, the proposed method is evaluated with relatively good accuracy. Moreover, improvements of adjustments from annual temperature dynamics on the proposed method are further discussed. Generally, the present method is a promising method for reconstructing LST with high spatiotemporal resolution at large scales benefiting from its simplicity and efficiency, relatively high accuracy, and seamless reconstruction.

Acknowledgment

The authors would like to thank Center for Geodata and Analysis, Faculty of Geographical Science, and Beijing Normal University for the high-performance computing support.

References

[1] Z.-L. Li *et al.*, "Satellite-derived land surface temperature: Current status and perspectives," *Remote Sens. Environ*., vol. 131, pp. 14–37, 2013.

[2] S.-B. Duan, Z.-L. Li, and P. Leng, "A framework for the retrieval of all-weather land surface temperature at a high spatial resolution from polar-orbiting thermal infrared and passive microwave data," *Remote Sens. Environ*., vol. 195, pp. 107–117, 2017.

[3] M. Anderson, J. Norman, W. Kustas, R. Houborg, P. Starks, and N. Agam, "A thermal-based remote sensing technique for routine mapping of land-surface carbon, water and energy fluxes from field to regional scales," *Remote Sens. Environ*., vol. 112, no. 12, pp. 4227–4241, 2008.

[4] W. Kustas and M. Anderson, "Advances in thermal infrared remote sensing for land surface modeling," *Agric. Forest Meteorol.*, vol. 149, no. 12, pp. 2071–2081, 2009.

[5] J. A. Sobrino, F. Del Frate, M. Drusch, J. C. Jimenez-Munoz, P. Manunta, and A. Regan, "Review of thermal infrared applications and requirements for future high-resolution sensors," *IEEE Trans. Geosci. Remote Sens.*, vol. 54, no. 5, pp. 2963–2972, May 2016.

[6] J. L. White-Newsome *et al.*, "Validating satellite-derived land surface temperature with *in situ* measurements: A public health perspective," *Environ. Health Perspect*., vol. 121, no. 8, pp. 925–31, Aug. 2013.

[7] M. G. Estes Jr. *et al.*, "Use of remotely sensed data to evaluate the relationship between living environment and blood pressure," *Environ. Health Perspect.*, vol. 117, no. 12, pp. 1832–8, Dec. 2009.

[8] P. Fu, "Responses of vegetation productivity to temperature trends over continental united states from MODIS imagery," *IEEE J. Sel. Top. Appl. Earth Obs. Remote Sens.*, vol. 12, no. 4, pp. 1085–1090, Apr. 2019.

[9] K. Liu, H. Su, X. Li, W. Wang, L. Yang, and H. Liang, "Quantifying spatial–temporal pattern of urban heat island in Beijing: An Improved assessment using land surface temperature (LST) Time series observations from LANDSAT, MODIS, and Chinese new satellite Gaofen-1," *IEEE J. Sel. Top. Appl. Earth Obs. Remote Sens.*, vol. 9, no. 5, pp. 2028–2042, May 2016.

[10] S.-B. Duan *et al.*, "Validation of collection 6 MODIS land surface temperature product using *in situ* measurements," *Remote Sens. Environ*., vol. 225, pp. 16–29, 2019.

[11] Q. Weng, "Thermal infrared remote sensing for urban climate and environmental studies: Methods, applications, and trends," *ISPRS J. Photogramm. Remote Sens.*, vol. 64, no. 4, pp. 335–344, 2009.

[12] Y. Wang, H. Du, Y. Xu, D. Lu, X. Wang, and Z. Guo, "Temporal and spatial variation relationship and influence factors on surface urban heat island and ozone pollution in the Yangtze River Delta, China," *Sci. Total Environ*., vol. 631–632, pp. 921–933, Aug 2018.

[13] P. Fu and Q. Weng, "Variability in annual temperature cycle in the urban areas of the United States as revealed by MODIS imagery," *ISPRS J. Photogramm. Remote Sens*., vol. 146, pp. 65–73, 2018.

[14] S. S. Peng *et al.*, "Afforestation in China cools local land surface temperature," *Proc. Natl. Acad. Sci.*, vol. 111, no. 8, pp. 2915–2919, Feb 2014.

[15] X. Li, Y. Zhou, G. R. Asrar, and Z. Zhu, "Creating a seamless 1 km resolution daily land surface temperature dataset for urban and surrounding areas in the conterminous United States," *Remote Sens. Environ*., vol. 206, pp. 84–97, 2018.

[16] X. Zhang, J. Zhou, F.-M. Gottsche, W. Zhan, S. Liu, and R. Cao, "A method based on temporal component decomposition for estimating 1-km all-weather land surface temperature by merging satellite thermal infrared and passive microwave observations," *IEEE Trans. Geosci. Remote Sens.*, vol. 57, no. 7, pp. 4670–4691, 2019.

[17] L. Lu, V. Venus, A. Skidmore, T. Wang, and G. Luo, "Estimating land-surface temperature under clouds using MSG/SEVIRI observations," *Int. J. Appl. Earth. Obs. Geoinf.*, vol. 13, no. 2, pp. 265–276, Jul. 2011.

[18] Z. Liu *et al.*, "Balancing prediction accuracy and generalization ability: A hybrid framework for modelling the annual dynamics of satellite-derived land surface temperatures," *ISPRS J. Photogramm. Remote Sens*., vol. 151, pp. 189–206, 2019.

[19] J. Lai *et al.*, "Does quality control matter? Surface urban heat island intensity variations estimated by satellite-derived land surface temperature products," *ISPRS J. Photogramm. Remote Sens.*, vol. 139, pp. 212–227, 2018.

[20] L. Sun *et al.*, "Reconstructing daily clear-sky land surface temperature for cloudy regions from MODIS data," *Comput. Geosci.*, vol. 105, pp. 10–20, 2017.

[21] P. Wu, Z. Yin, H. Yang, Y. Wu, and X. Ma, "Reconstructing geostationary satellite land surface temperature imagery based on a multiscale feature connected convolutional neural network," *Remote Sens*., vol. 11, no. 3, 2019.

[22] D. Long *et al.*, "Generation of MODIS-like land surface temperatures under all-weather conditions based on a data fusion approach," *Remote Sens. Environ*., vol. 246, 2020, Art. no. 111863.

[23] H. R. Shwetha and D. N. Kumar, "Prediction of high spatio-temporal resolution land surface temperature under cloudy conditions using microwave vegetation index and ANN," *ISPRS J. Photogramm. Remote Sens*., vol. 117, pp. 40–55, 2016.

[24] X. Kou, L. Jiang, Y. Bo, S. Yan, and L. Chai, "Estimation of land surface temperature through blending MODIS and AMSR-E data with the bayesian maximum entropy method," *Remote Sens*., vol. 8, no. 2, 2016, Art. no. 105.

[25] S. Xu, J. Cheng, and Q. Zhang, "Reconstructing all-weather land surface temperature using the Bayesian maximum entropy method over the Tibetan Plateau and Heihe River Basin," *IEEE J. Sel. Top. Appl. Earth. Obs. Remote Sens.*, vol. 12, no. 9, pp. 3307–3316, Sep. 2019.
[26] T. R. H. Holmes, W. T. Crow, and C. Hain, "Spatial patterns in timing of the diurnal temperature cycle," *Hydrol. Earth Syst. Sci.*, vol. 10, no. 5, pp. 6019–6048, 2013.
[27] T. R. H. Holmes, W. T. Crow, C. Hain, M. C. Anderson, and W. P. Kustas, "Diurnal temperature cycle as observed by thermal infrared and microwave radiometers," *Remote Sens. Environ*., vol. 158, pp. 110–125, 2015.
[28] F. Aires, C. Prigent, W. B. Rossow, and M. Rothstein, "A new neural network approach including first guess for retrieval of atmospheric water vapor, cloud liquid water path, surface temperature, and emissivities over land from satellite microwave observations," *J. Geophys. Res. Atmos.*, vol. 106, no. D14, pp. 14887–14907, 2001.
[29] T. R. H. Holmes, R. A. M. De Jeu, M. Owe, and A. J. Dolman, "Land surface temperature from Ka band (37 GHz) passive microwave observations," *J. Geophys. Res. Atmos*., vol. 114, no. D4, 2009.
[30] F. Aires, C. Prigent, and W. B. Rossow, "Temporal interpolation of global surface skin temperature diurnal cycle over land under clear and cloudy conditions," *J. Geophys. Res. Atmos*., vol. 109, no. D4, 2004.
[31] M. Owe and A. Van De Griend, "On the relationship between thermodynamic surface temperature and high-frequency (37 GHz) vertically polarized brightness temperature under semi-arid conditions," *Int. J. Remote Sens.*, vol. 22, no. 17, pp. 3521–3532, 2001.
[32] J. Zhou, F. Dai, X. Zhang, S. Zhao, and M. Li, "Developing a temporally land cover-based look-up table (TL-LUT) method for estimating land surface temperature based on AMSR-E data over the Chinese landmass," *Int. J. Appl. Earth Obs. Geoinf*., vol. 34, pp. 35–50, 2015.
[33] S.-S. Chen, X.-Z. Chen, W.-Q. Chen, Y.-X. Su, and D. Li, "A simple retrieval method of land surface temperature from AMSR-E passive microwave data—A case study over Southern China during the strong snow disaster of 2008," *Int. J. Appl. Earth Obs. Geoinf.*, vol. 13, no. 1, pp. 140–151, 2011.
[34] C. Yoo, J. Im, D. Cho, N. Yokoya, J. Xia, and B. Bechtel, "Estimation of all-weather 1 km MODIS land surface temperature for humid summer days," *Remote Sens.*, vol. 12, no. 9, pp. 1398–1421, 2020.
[35] P. Fu, Y. Xie, Q. Weng, S. Myint, K. Meacham-Hensold, and C. Bernacchi, "A physical model-based method for retrieving urban land surface temperatures under cloudy conditions," *Remote Sens. Environ*., vol. 230, pp. 111–191, 2019.
[36] M. Domrös and G. Peng, *The Climate of China*. New York, NY, USA: Springer, 2012.
[37] Z. Wan and J. Dozier, "A generalized split-window algorithm for retrieving land-surface temperature from space," *IEEE Trans. Geosci. Remote Sens.*, vol. 34, no. 4, pp. 892–905, Jul. 1996.
[38] Z. Wan, "New refinements and validation of the MODIS land-surface temperature/emissivity products," *Remote Sens. Environ*., vol. 112, no. 1, pp. 59–74, 2008.
[39] Z. Wan, "New refinements and validation of the collection-6 MODIS land-surface temperature/emissivity product," *Remote Sens. Environ*., vol. 140, pp. 36–45, 2014.
[40] C. Huang *et al.*, "Intercomparison of AMSR2- and MODIS-derived land surface temperature under clear-sky conditions," *IEEE J. Sel. Top. Appl. Earth Obs. Remote Sens*., vol. 12, pp. 3286–3294, Sep. 2019.
[41] G. Balsamo *et al.*, "ERA-5 and ERA-Interim driven ISBA land surface model simulations: Which one performs better?" *Hydrol Earth Syst. Sci.*, vol. 22, no. 6, pp. 3515–3532, 2018.
[42] J. Lai *et al.*, "Identification of typical diurnal patterns for clear-sky climatology of surface urban heat islands," *Remote Sens. Environ*., vol. 217, pp. 203–220, 2018.
[43] H. Li *et al.*, "Evaluation of the VIIRS and MODIS LST products in an arid area of Northwest China," *Remote Sens. Environ*., vol. 142, pp. 111–121, 2014.
[44] J. Jiang *et al.*, "Evaluation of land surface temperature retrieval from FY-3B/VIRR data in an arid area of northwestern China," *Remote Sens*., vol. 7, no. 6, pp. 7080–7104, 2015.
[45] J. B. Adams *et al.*, "Classification of multispectral images based on fractions of endmembers: Application to land-cover change in the Brazilian Amazon," *Remote Sens. Environ*., vol. 52, no. 2, pp. 137–154, 1995.
[46] Z. Zou *et al.*, "Enhanced modeling of annual temperature cycles with temporally discrete remotely sensed thermal observations," *Remote Sens*., vol. 10, no. 4, 2018, Art. no. 650.
[47] E. J. Good, "An in situ-based analysis of the relationship between land surface "skin" and screen-level air temperatures," *J. Geophys. Res. Atmos.*, vol. 121, no. 15, pp. 8801–8819, 2016.
[48] L. Breiman, "Random forests," *Mach. Learn.*, vol. 45, no. 1, pp. 5–32, 2001.
[49] M. Fily, "A simple retrieval method for land surface temperature and fraction of water surface determination from satellite microwave brightness temperatures in sub-arctic areas," *Remote Sens. Environ*., vol. 85, no. 3, pp. 328–338, 2003.
[50] C. Prigent, C. Jimenez, and F. Aires, "Toward "all weather," long record, and real-time land surface temperature retrievals from microwave satellite observations," *J. Geophys. Res. Atmos.*, vol. 121, no. 10, pp. 5699–5717, 2016.

Kangning Li received the B.S. degree in geographic information system from the College of Urban and Environmental Science, Northwest University, Xi'an, China, in 2016. She is currently working toward the Ph.D. degree with the State Key Laboratory of Remote Sensing Science, Faculty of Geographical Science, Beijing Normal University, Beijing, China. Her research interests include thermal remote sensing of urban environment.

Yunhao Chen received the B.S. and M.S. degrees in resource management from the Anhui University of Science and Technology, Huainan, China, in 1994 and 1997, respectively, and the Ph.D. degree in geodetic engineering from the China University of Mining and Technology, Beijing, China, in 1999.

From 2000 to 2001, he was a Postdoctoral Research with Beijing Normal University, Beijing. Since 2001, he has been with the Faculty of Geographical Science, Beijing Normal University, where he is currently a Professor with the State Key Laboratory of Remote Sensing Science. His research interests include thermal remote sensing of urban environment and applications of remote sensing in ecology.

Haiping Xia received the B.S. degree in geographic information system from the School of Environment Science and Spatial Informatics, China University of Mining and Technology, Xuzhou, China, in 2015. She is currently working toward the Ph.D. degree with the State Key Laboratory of Remote Sensing Science, Faculty of Geographical Science, Beijing Normal University, Beijing, China. Her research interests include thermal sharpening and analysis on urban thermal environment.

Adu Gong received the B.S. degree in land use and land planning from Southwest University, Chongqing, China, in 1998, the M.S. degree in soil and water conservation from Chinese Academy of Sciences/Ministry of Water Resources Chengdu Institute of Mountain Hazards and Environment, Chengdu, China, in 2001, and the Ph.D. degree in geography from Beijing Normal University, Beijing, China, in 2005.

He is currently an Associate Professor with the Faculty of Geographical Science and State Key Laboratory of Remote Sensing Science, Beijing Normal University, Beijing, China. His research interests include thermal remote sensing and urban heat island.

Zheng Guo received the B.S. degree in horticultural from China Agricultural University, Beijing, China, in 2007, the M.S. degree in ecology from Zhejiang A&F University, Zhejiang, China, in 2010, and the Ph.D. degree in geography from Beijing Normal University, Beijing, China, in 2013.

He is a Senior Engineer with the Division of Remote Sensing Data Application, National Satellite Meteorological Center, China Meteorological Administration, Beijing, China. His research interests include thermal remote sensing and applications for thermal environment of the city and atmospheric pollutants monitored by remote sensing.